

# Matched photometric catalogs of GALEX UV sources with Gaia DR2 and SDSS DR14 databases (GUVmatch)

Luciana Bianchi<sup>1</sup> and Bernard Shiao<sup>2</sup>

bianchi@jhu.edu

Received \_\_\_\_\_; accepted \_\_\_\_\_

---

<sup>1</sup>Dept. of Physics & Astronomy, The Johns Hopkins University, 3400 N. Charles St., Baltimore, MD 21218, USA; <http://dolomiti.pha.jhu.edu>

<sup>2</sup>Space Telescope Science Institute, 3400 San Martin Dr., Baltimore, MD 21210

## ABSTRACT

We have matched the ultraviolet (UV) sources in *GUVcat\_AIS* (Bianchi et al. 2017, 2020a) with optical databases having similar depth and wide sky coverage. *GUVcat\_AIS* has GALEX far-UV (FUV,  $\lambda_{eff} \sim 1528\text{\AA}$ ) and near-UV (NUV,  $\lambda_{eff} \sim 2310\text{\AA}$ ) photometry of  $\approx 83$  million sources, covering 24,788 square degrees of the sky, with typical depth of FUV=19.9, NUV=20.8 ABmag. Matches with Gaia and SDSS databases are presented here.

Gaia data release 2 (DR2), covering the entire *GUVcat* footprint (Bianchi et al. 2019), detected about one third of the *GUVcat\_AIS* sources. We found 31,925,294 Gaia DR2 counterparts to 30,024,791 *GUVcat\_AIS* unique sources, with photometry in *Gaia* *G* band, and often also in *Gaia* *BP* and *RP* bands; 26,275,572 matches have a parallax measurement, 21,084,628 / 18,588,140 / 16,357,505 with parallax error less than 50%/30%/20%.

The match with SDSS data release 14 (DR14) yields 23,310,532 counterparts to 22,207,563 unique *GUVcat\_AIS* sources, 10,167,460 of which are point-like, over a total overlap area of  $\approx 11,100$  square degrees (Bianchi et al. 2019). SDSS adds to the UV photometry five optical magnitudes: *u*, *g*, *r*, *i*, *z*, and optical spectra of 860,224 matched sources.

We used a match radius of  $3''$ , consistent with previous works (e.g., Bianchi et al. (2011a)), although the positions agree to  $\lesssim 1.5''$  for the majority of [point-like] matched-sources, in order to identify possible multiple matches whose UV flux could be unresolved in GALEX imaging. The catalogs can be trimmed to a tighter match radius using the provided separation.

The multi-band photometry is used to identify classes of astrophysical objects that are prominent in UV, to characterize the content of the *GUVmatch* catalogs, where stars in different evolutionary stages, QSOs, and galaxies can be separated.

*Subject headings:* Astronomy Databases: surveys, catalogs, virtual observatory tools, miscellaneous; Stars: statistics, white dwarfs, early-type ; Galaxies: statistics; (Sources:) Ultraviolet:stars, galaxies, general, ISM; The Galaxy: stellar content, structure

## 1. Introduction.

### 1.1. The catalog of UV sources *GUVcat*

To facilitate statistical studies of UV sources, Bianchi et al. (2017)(revised 2020) constructed *GUVcat\_AIS*, a catalog of  $\sim 83$  million GALEX<sup>1</sup> unique UV sources, by removing duplicate measurements from repeated observations of the same source. The GALEX All-sky Imaging Survey (AIS) consists of 57,000 distinct imaging observations (“visits”) of over 28,700 fields. To build *GUVcat\_AIS*, Bianchi et al. (2017) used both “co-adds” and “visits”, in order to cure some incorrect associations (“co-adds”) of same-field visits in the original GALEX pipeline processing. See Bianchi et al. (2017) for details, and for description of other caveats. *GUVcat\_AIS* supersedes earlier versions of unique UV source catalogs constructed from previous data releases, such as the widely used *BCScat* (Bianchi et al. 2014) and the earlier catalogs of Bianchi et al. (2011a,b).

In *GUVcat* only one measurement for each UV source is retained (unique source list), and the field edges, that are plagued with artifacts, are trimmed. *GUVcat\_AIS\_FOV055* contains all sources within  $0.55^\circ$  of the field center, and eliminates most rim artifacts without loss of real sources (cfr Bianchi et al. (2017)). *GUVcat*, alone or matched with surveys at other wavelengths, enables effective selection of UV-source samples (e.g., Bianchi et al. (2007, 2011a, 2018b)). The power to identify and characterize astrophysical sources is maximized when the UV measurements are complemented with optical-IR data (e.g., Bianchi et al. (2011a,b); Bianchi (2009); Bianchi et al. (2009, 2007, 2005); Hutchings &

---

<sup>1</sup>The Galaxy Evolution Explorer (GALEX, Martin et al. (2005)) operated from July 2003 to Feb. 2012, surveying the sky simultaneously in FUV and NUV, until the FUV detector stopped working in 2009. A total of almost 600 million individual source measurements are in the GALEX database (Bianchi 2009, 2011, 2014)

Bianchi (2010a,b); Smith et al. (2014)). In order to match two databases, unique-source catalogs must be used for each (no repeated entries for the same source). Currently, for GALEX this is only possible using *GUVcat*, while the original database<sup>2</sup> includes repeated measurements, that are instead useful for serendipitous variability searches (e.g., Conti et al. (2014); de la Vega & Bianchi (2018) and references therein). *GUVcat\_AIS* includes all fields observed with both FUV and NUV detectors in the All-sky Imaging Survey (AIS), the survey with the widest sky coverage (see Figure 1 of Bianchi et al. (2017), and Bianchi et al. (2014) for more maps; also Bianchi (2009) for an overview). By excluding the observations that have only the NUV detector exposed (cfr Figure 1-left of Bianchi et al. (2017)) we ensure that the statistics of samples selected by criteria including the FUV-NUV color is unbiased.

*GUVcat\_AIS\_FOV055* (Bianchi et al. (2017), revised by Bianchi et al. (2020a)) contains 82,992,086 unique UV sources, over an area of 24,790 square degrees (Bianchi et al. 2019). Coverage is scant at low Galactic latitudes, due to the abundance of UV-bright hot stars near the Galactic plane that would violate the countrate safety limits of GALEX detectors, as shown in Figure 1 of Bianchi et al. (2017). The tags (columns) included in *GUVcat\_AIS* are described in Table 8 of Bianchi et al. (2017). Among the tags constructed in addition to those provided by the GALEX pipeline, we recall two of interest here: INLARGEOBJ and LARGEOBJSIZE. They indicate whether a UV source is inside the footprint of an extended object such as a nearby galaxy or dense stellar cluster<sup>3</sup> (and, if so, the size of the extended object), where quality of source detection, characterization and measurement can be highly compromised, as illustrated clearly in Figure 5 of Bianchi et al. (2017).

*GUVcat\_AIS* has a typical depth of FUV=19.9, NUV=20.8 ABmags. The fraction

---

<sup>2</sup>hosted at MAST: <https://galex.stsci.edu>

<sup>3</sup>if so, INLARGEOBJ is not 'N' and LARGEOBJSIZE is >0.

of NUV sources that have a significant detection also in FUV varies between a few % and  $\sim 15\%$  overall from low to high Galactic latitudes, but it also varies significantly with source brightness (Bianchi et al. 2011b, 2017). In total, about 10% of the  $\sim 83$  million *GUVcat\_AIS* sources have a significant FUV detection.

The ratio of FUV detections over NUV detections decreases towards low latitudes, but it actually increases towards the Galactic plane for the brighter sources, as expected since these are mostly hot stars (see Figure 2 of Bianchi et al. (2011b) and Figure 6 of Bianchi et al. (2017)). The overall decrease is due to the numerous faint sources, mostly extra-Galactic (QSOs for the point-like sources), whose intrinsic density does not depend on Galactic coordinates but whose detection is affected by the severe extinction by dust near the Galactic plane (Figures 2 and 5 of Bianchi et al. (2011b)), and whose FUV-NUV color varies with red-shift and therefore also with observed magnitude (e.g., Section 3, also Figures 3-5 of Bianchi (2009), Figure 5 of Bianchi et al. (2011a)). UV source densities, by magnitude and by color, at varying Galactic latitudes, are shown for *GUVcat\_AIS* in Figure 6 of Bianchi et al. (2017), and in form of illustrative sky maps by Bianchi et al. (2014).

## 1.2. Choice of match radius. Accounting for multiple matches.

We matched *GUVcat\_AIS\_FOV055* with the major optical surveys currently available, the Sloan Digital Sky Survey (SDSS, Gunn et al. (1998)) data release 14 (DR14, Abolfathi et al. (2018)), and Gaia data release 2 (DR2, Gaia collaboration et al. (2018)). A forthcoming work will present the match with Pan-STARRS PS1  $3\pi$  survey (Chambers et al. (2016)). For each survey, the characteristics that are relevant to our purpose are summarized in separate sections below.

We note here a general consideration of consequence in any database matching, i.e. the

need to assess the appropriate match radius (maximum distance between source positions in the two catalogs for a source to be retained as a match) such to minimize the number of spurious matches and at the same time minimize the loss of real matches. These two criteria work in the opposite directions of favouring a more restricted match radius and a more generous one, respectively. Spatial resolution and position accuracy of the databases to be matched determine the optimum match radius, and the density of sources in the sky affects the incidence of spurious matches. GALEX’s spatial resolution is nominally  $4.2/5.2''$  (FUV/NUV, Morrissey et al. (2007)); it degrades towards the field edges. Nearly all sources in the outermost rim, where measurements of position and flux become problematic, are excluded from *GUVcat*. The coordinates of the source centroid in GALEX data releases GR6 / GR7 have a reported accuracy of  $0.35/0.48''$  (NUV/FUV) in GR6 and  $0.32/0.34''$  (NUV/FUV) in GR7<sup>4</sup>.

Ground-based surveys such as SDSS and Pan-STARRS have a typical spatial resolution of  $1.4''$ , that is, about 3 times higher than GALEX’s, and Gaia has a higher astrometric precision. On the other hand, UV-emitting sources are very rare, compared with the density of red or IR sources (for both Galactic and extra-Galactic objects), therefore most matches are unique and reliable (one-to-one). Nonetheless, due to the higher spatial resolution of the optical databases used here with respect to GALEX, when more than one optical counterpart to a UV source is found within the match radius, the UV flux could be composite of these optical counterparts, that are resolved e.g. by SDSS or Gaia but unresolved in GALEX imaging. In such cases, keeping only the closest match would be misleading, since the UV flux may be contaminated by a neighbor while the optical flux would be only the flux from the closest match, making UV–optical colors meaningless, and the analysis biased. In the case of multiple matches one can also look at the magnitudes

---

<sup>4</sup>[http://www.galex.caltech.edu/researcher/gr6\\_docs/GI\\_Doc\\_Ops7.pdf](http://www.galex.caltech.edu/researcher/gr6_docs/GI_Doc_Ops7.pdf)

and colors of the two (or more) counterparts, and if one counterpart is - for example - much redder and much fainter than another, it is likely that all or most of the UV flux originates from the hot, brighter one. However, if the UV source is an unresolved binary comprising a very hot star and a cooler one, the actual optical counterpart may have red optical colors because the flux at longer wavelengths is emitted mostly by the cool companion star (e.g., Bianchi et al. (2018b)).

To keep track of multiple matches, in order to enable a correct, unbiased scientific exploitation of the matched catalogs, we used a slightly generous match radius of  $3''$ , which is larger than the typical coordinate offsets between the matched databases, but allows us to identify the cases where two or more nearby optical sources may be unresolved by GALEX. To facilitate analysis, we created tags (similarly to Bianchi et al. (2011a,b)) by which multiple matches can be immediately identified. The definition of these tags is given in Table 1.

## 2. *GUVcat\_AIS* matches with optical catalogs

Below we describe the *GUVmatch* catalogs, i.e. *GUVcat* matched with Gaia DR2 and SDSS DR14. We estimate the incidence of spurious matches relative to a given match separation, and discuss the fraction of multiple matches. The content of sources in the *GUVmatch* catalogs in terms of broad astrophysical classes is discussed in Section 3.

### 2.1. *GUVcat\_AIS\_FOV055* match with Gaia DR2: *GUVmatch\_AISxGaiaDR2*

The Gaia mission covers the whole sky, accumulating scans with a pattern that results in progressive completeness as the survey continues (Brown 2018). We matched *GUVcat\_AIS\_FOV055* (Bianchi et al. 2017, 2020a) with Gaia’s data release 2 (DR2) (Gaia

Table 1. Tags to identify multiple matches within the match radius

Tag	Meaning and Values
DSTARCSEC	distance in arcsec between the UV source position and the matched-source position
DISTANCERANK	= 0 : this is the only match to this UV source = 1 : this is the closest of more than one match to this UV source =n>1 : the n <sup>th</sup> match to the same UV source, ranked by distance
MULTIPLEMATCHCOUNT	# of matches found for this UV source (by definition, equal to max(DISTANCERANK) + 1)
REVERSEDISTANCERANK <sup>a</sup>	= 0 if the matched source matches only this one UV source = 1 if the matched source matches also other UV sources, and this is the closest match =n>1 : the n <sup>th</sup> match of this optical source to different UV sources
REVERSEMULTIPLEMATCHCOUNT <sup>a</sup>	how many UV sources are matched by this optical source

<sup>a</sup>these are very rare occurrences, see statistics in Tables 3 and 4

Table 2. Vega to AB mag Conversion

Filter	Vega - AB
GALEX FUV	-2.223
GALEX NUV	-1.699
SDSS u	-0.944
SDSS g	0.116
SDSS r	-0.131
SDSS i	-0.354
SDSS z	-0.524
PanSTARRS gp1	0.103
PanSTARRS rp1	-0.133
PanSTARRS ip1	-0.361
PanSTARRS zp1	-0.516
PanSTARRS yp1	-0.543
PanSTARRS wp1	-0.084
Gaia DR2 G	-0.092
Gaia DR2 G_BP	-0.066
Gaia DR2 G_RP	-0.362
Gaia DR2 G rev <sup>a</sup>	-0.079
Gaia DR2 G_BP rev <sup>a</sup>	-0.073
Gaia DR2 G_RP rev <sup>a</sup>	-0.356

<sup>a</sup>For Gaia, the first set of values are computed with the passbands used in the Gaia DR2 database, the “rev” values are computed with the revised set of G, G\_BP and G\_RP passbands based on a later available nominal knowledge of the instrument, published by Evans et al. (2018).

collaboration et al. 2018). A space-borne instrument designed for precision astrometry, Gaia has much higher resolution than *GALEX* and than the ground-based optical survey used here, but some UV-bright objects detected by GALEX are below Gaia’s detection limits in Gaia’s optical bands, and only about one third of the *GUVcat* sources have a match in Gaia DR2.

Table 3 provides a statistical overview to characterize the matched catalog at a glance. For the total matched catalog, and for  $5^\circ$  Galactic latitude strips, we give the total number of matches, i.e. all Gaia DR2 distinct sources found within the  $3''$  match radius around the UV sources<sup>5</sup>, the number of UV sources with Gaia counterparts, and of those with a unique Gaia match (tag *DISTANCERANK* = 0), and the fraction of UV sources that have multiple Gaia matches. The second row, for each Galactic latitude range, gives the counts excluding sources that fall in the footprint of extended objects larger than  $30'$ . This overview is useful because one can examine characteristics (e.g., color distributions) of clean samples by selecting sources with a unique match, and then correct the resulting statistics for the discarded fraction of multiple-match sources. All Gaia DR2 sources have a flux measurement in at least the *Gaia G* band, with additional measurements in *Gaia BP* and *Gaia RP*; not all Gaia DR2 sources have a significant parallax, since the [parallax, proper motion] solution requires a sufficient number of repeated measurements and a successful fit to the data. In Table 3 we list also the number of Gaia matches that have a parallax measurement (excluding the parallaxes with negative values, that are a clear indication of solution failure), and of those that have parallax error  $\leq 20/30/50\%$

---

<sup>5</sup>in the matched catalog, a UV source with *n* matches is entered *n* times (one row for each distinct match); a unique list of sources can be immediately derived by selecting entries with tag *DISTANCERANK* <2 (Table 1); a list of sources with only one match can be extracted by selecting *DISTANCERANK* = 0

(counted from the unique UV source list, column 3 of Table 3). For comparison, the number of UV *GUVcat*\_AIS sources and the area covered at different Galactic latitudes is given in Tables 6 and 7 of Bianchi et al. (2017). Of the UV sources with Gaia matches, 1,977,196 have significant FUV detection (with a total of 2,100,359 Gaia matches), of which 1,145,775/686,339/283,448 have errors  $< 0.3/0.2/0.1$  mag in both FUV and NUV.

Figure 1 shows the distribution of matched-sources separation, i.e. the difference between the *GUVcat* and Gaia DR2 position (tag *DSTARCSEC* in the matched catalog). For nearby objects, if they have a high proper motion, part of the difference may also be ascribed to actual source motion in the plane of the sky<sup>6</sup>, although most UV GALEX sources are probably rather distant (see e.g., Bianchi et al. (2011a, 2018b) and Figure 2). Gaia, given its spatial resolution, and its main objective and corresponding mission design, has a superior astrometry with respect to GALEX; however, an important caveat must be recalled concerning sources in close binaries. Whether real binaries or chance alignments along the line of sight, Gaia’s pipeline - in DR2 - does not solve for pairs closer than  $2''$ . According to the current documentation, if two sources closer than  $2''$  are detected, only one is kept, but not necessarily the same one throughout the repeated observations, potentially hampering the [parallax, proper motion] solution. This caveat affects probably a very small number of sources, especially considering that our starting point is a catalog of

---

<sup>6</sup>the measurements in *GUVcat* may have been taken at any time during GALEX operations with both detectors; the observing date of each entry can be found by searching for the “OBJID” identifier in the Casjobs Visit-level (if “CORV” = V) or MCAT-level (if “CORV” = C) tables, and retrieving the additional tags of that measurement; GALEX coordinates are given at a reference epoch of 2000., equinox = 2000. Gaia DR2 (<https://www.cosmos.esa.int/web/gaia/dr2>) is built from data collected between 25 July 2014 and 23 May 2016; the reference epoch is J2015.5.

UV sources, rather sparse in comparison to the density of optical sources. It is, however, relevant for some specific science goals, such as for example our study of hot white dwarfs in binaries (e.g., Bianchi et al. (2011a, 2018b), see Section 3). As recalled in Section 1.1, the centroid position of *GALEX* sources is as good as 0.32-0.35/0.34-0.48'' (NUV/FUV) in GR6/7, except possibly in the periphery of the fields. Therefore, if we were to restrict the sample to matches within a smaller match radius (as can be easily accomplished by applying a restriction in tag *DSTARCSEC* in our catalog), we might gain by eliminating some spurious secondary matches, but at the price of possibly losing binaries and high proper motion objects.

To estimate the incidence of spurious matches, i.e. accidental positional coincidences, we performed a test by matching Gaia DR2 with a fake *GUVcat*-like catalog, made by picking one every ten *GUVcat* sources, and offsetting their position by 5arcmin. The  $\gtrsim 8$  million sources “fake-*GUVcat*” catalog has 252,135 Gaia DR2 matches; their distribution with separation (difference between the position of the *GALEX* source and that of the Gaia match) is also shown in Figure 1 (brown histogram). For a consistent comparison with the actual catalog, the result of the “fake-*GUVcat*” match is multiplied by 10, because we used a one-tenth fake *GUVcat* catalog. The number of matches per bin increases with separation because the annuli with increasing radius cover a progressively larger area; we do not expect random matches to favour small separations. Figure 1 shows that at a separation of 3'' (the chosen match radius), the number of spurious matches almost reaches the number of matches to the real *GUVcat* positions. Therefore, we can consider our catalog rather complete (no real counterparts beyond the matched radius, for point-like sources). Figure 1 also shows that the secondary matches (the additional matches with separation larger than that of the closest match) could be mostly random alignments; but even though the closest match may be the [only] real counterpart, the UV flux can be composite of the primary and secondary match, given the *GALEX* resolution, as discussed earlier. Therefore, sources

with multiple matches should be examined with care.

The Gaia DR2 database gives Gaia magnitudes in the Vega magnitude system. We kept the original magnitude values in *GUVmatch\_AISxGaiaDR2*. Therefore, in *GUVmatch\_AISxGaiaDR2*, GALEX’s FUV and NUV magnitudes are AB mags, and Gaia G, BP, RP are Vega mags; for SED analysis they must be converted to one of the two systems, by applying to one of the two sets the transformation coefficients taken from Table 2 or other sources. We provide in Table 2 the transformation coefficients between Vega and AB magnitude systems, calculated using the Vega spectrum and the transmission curves for all filters included in our catalogs. For Gaia DR2, we calculated the coefficients with the transmission curves used by the Gaia project for the DR2 photometry released in 2018, and also with the revised curves published by Evans et al. (2018). Other revisions are published, as inflight instrumental response functions continue to be investigated and refined; an updated summary is given in the Gaia documentation pages, <https://www.cosmos.esa.int/web/gaia/dr2-known-issues#PhotometrySystematicEffectsAndResponseCurves>. Our computed Gaia conversion coefficients are not identical to the zero-point differences reported in the Gaia online documentation<sup>7</sup>, the differences are up to  $\approx 4$  hundredths of a magnitude, and are probably due to the interpolation of the transmission curves downloaded and the adopted Vega spectrum.

Figure 2 shows the distribution of distances, derived from Gaia parallax<sup>8</sup>, for the matched Gaia DR2 UV sources that have parallax error less than 50%. Because the sources with FUV detection are only about one tenth of the NUV detections, we show also an

---

<sup>7</sup>[https://gea.esac.esa.int/archive/documentation/GDR2/Data\\_processing/chap\\_cu5pho/sec\\_cu5pho\\_calibr/ssec\\_cu5pho\\_calibr\\_extern.html](https://gea.esac.esa.int/archive/documentation/GDR2/Data_processing/chap_cu5pho/sec_cu5pho_calibr/ssec_cu5pho_calibr_extern.html), see Tables 5.2 and 5.3 in that section.

<sup>8</sup>we added to the parallax a bias of 0.052 mas, following Shoenrich et al. (2019)

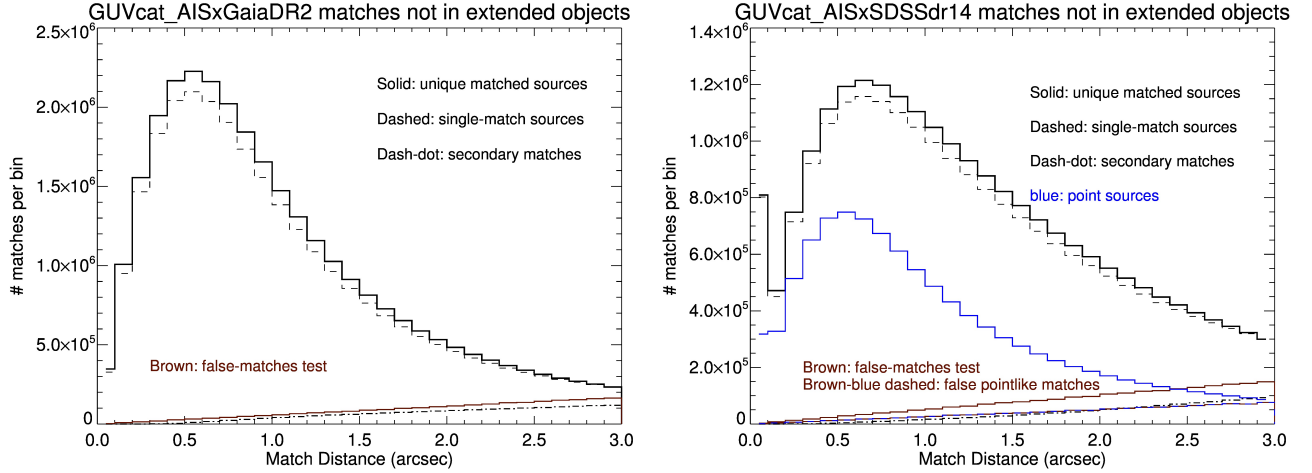


Fig. 1.— Distribution of separation between the *GUVcat\_AIS* UV-source position and the matched-source position (Gaia DR2, left panel; SDSS DR14, right panel). The distributions of the entire matched catalogs (counting the UV sources only once, solid line), and the sources with a unique match (dashed line) are qualitatively similar, because multiple matches are a small fraction (Section 1, Tables 3 and 4). The separation distribution of primary matches peaks at values around  $0.6''$ , while that of the secondary matches (dash-dot line) increases towards larger separations. For the SDSS matches, point-like sources are also shown separately (blue histogram), since extended sources may have a looser definition of source center across the wavelengths. To assess the fraction of spurious matches, we matched each optical database with a replica of *GUVcat\_AIS* with altered coordinates; the distribution of false matches is shown in brown. In the counts, we excluded sources in extended objects such as galaxies or stellar clusters larger than  $30\text{arcmin}$  (see Bianchi et al. (2017)).

expanded view of the FUV-detected sources within  $1500\text{ pc}$ . We also separate the sample in “hotter” and “cooler” sources, according to their FUV-NUV color of  $<0$  or  $>0$  respectively. For stars, the GALEX FUV-NUV color is a good indicator of stellar temperature, since it is almost reddening-free for typical Milky Way (MW) dust with  $R_V = 3.1$  (Bianchi et al. (2017), their Table 1, see also Section 3). The cut at FUV-NUV=0 separates stars hotter

than  $\sim 20,000$  K (the exact value depending on gravity and metallicity) from cooler stars and from the majority of extra-Galactic sources. To separate single hot stars from binaries, which is one of our motivations for building these matched catalogs, and cooler stars from extra-Galactic sources, different color combinations are useful, as shown in Section 3 (see also e.g., Bianchi (2009); Bianchi et al. (2011a) for additional discussion).

A higher fraction of the “cooler” UV sources have Gaia parallaxes than the hotter ones, as can be expected because very hot stars are optically fainter than cooler stars with similar UV brightness, as will be illustrated in Section 3. We point out that, because the FUV-NUV color requires a detection in both filters, and the fraction of sources with FUV detections is about one tenth of the *GUVcat* total NUV sample overall, the fraction of “hotter” and “cooler” stars shown in Figure 2 is a small subset of the total *GUVmatch\_AISxGaiaDR2* sample; the number of sources with good parallax measurements increases further for NUV sources undetected in FUV, that are cooler yet.

## 2.2. *GUVcat\_AIS\_FOV055* match with SDSS DR14:

### *GUVmatch\_AISxSDSSdr14*

The Sloan Digital Sky Survey (SDSS, Gunn et al. (1998)) provides five-band  $u$ ,  $g$ ,  $r$ ,  $i$ ,  $z$  photometry over a large part of the northern sky. The overlap with the *GUVcat\_AIS* footprint is shown in Figure 1 of Bianchi et al. (2014) in Galactic coordinates. The figure is not repeated here as the difference with respect to earlier releases will not be appreciable. The total current overlap is  $\sim 11,100$  square degrees (Table 1 of Bianchi et al. (2019)); the area of overlap in any chosen region of the sky can be calculated with the online tool

*AREAc*<sup>9</sup> (Bianchi et al. 2019). The match with SDSS data release 14 (DR14<sup>10</sup>, Abolfathi et al. (2018)) yields 23,310,532 counterparts within 3'' of 22,207,563 unique *GUVcat*\_AIS sources, 10,167,460 of which are point-like according to the SDSS pipeline photometry. SDSS spectra exist for 860,224 matched UV sources. In the SDSS DR14 database, some sources with the same photometric identifier are repeated because two spectra exist; there are 21 such repeats in the resulting matches, for these we kept only one entry, for the sake of counting how many unique *GUVcat* sources have matches. Therefore, only one of the available SDSS spectra is listed for these cases. *GUVcat* starting point is a list of all sources detected in NUV, regardless of FUV detection; among the matched sources, 3,511,890 have also significant detection in GALEX-FUV, of these 1126671 / 427361 / 103077 have error less than 0.3/0.2/0.1 mag in both FUV and NUV.

More statistical figures are given in Table 4, reported for the entire matched database and by Galactic latitudes.<sup>11</sup> As in Table 3, the second row for each Galactic latitude range gives the source counts, excluding sources that fall in the footprint of extended objects larger than 30'. Due to the scant sky coverage of the UV surveys near the Galactic plane, and the significant drop in UV source measurements at very low Galactic latitudes because of dust extinction, as shown dramatically in Figure 2 of Bianchi et al. (2011a), and to the SDSS footprint favouring the Northern latitudes (Figure 1 of Bianchi et al. (2014)), the number of SDSS DR14 matched sources significantly decreases at low Galactic latitudes, although the fraction of multiple matches increases, owing to the actual higher density of

---

<sup>9</sup><http://dolomiti.pha.jhu.edu/uvsky/area/AREAc.php>

<sup>10</sup><https://www.sdss.org/dr14/>

<sup>11</sup>the area of overlap between *GUVcat*\_AIS and SDSS DR14 by slices of Galactic latitude can again be found in Table 1 of Bianchi et al. (2019), or calculated with the *AREAc* tool for any desired region (<http://dolomiti.pha.jhu.edu/uvsky/area/AREAc.php>).

stars in the Milky Way disk. This is shown in Figure 3 of Bianchi et al. (2011a) for an earlier version of the matched catalog; although the present matched catalog is significantly expanded both in coverage and quality with respect to the 2011 version, and includes additional science-facilitating tags, we do not repeat the figure here because it would be very similar.

Figure 3 shows the distribution of *GUVmatch\_AISxSDSSdr14* sources in FUV, NUV, *u*, *g*, *r*, *i* magnitudes, color-coded by filter. As in Figure 2, for a cleaner sample, we excluded sources in extended objects larger than  $30'$ ; these are a very small fraction (Table 4) and do not change appreciably the histograms. For FUV and NUV, we also plot separately the counts for sources that have “point-like” morphology according to the SDSS pipeline (dashed-line histograms). As for the Gaia matched catalog (previous section), we also plot counts separating sources by FUV-NUV color; these are shown with pale red (FUV-NUV  $>0$ ) or fuchsia (FUV-NUV  $<0$ ) dashes mixed with indigo (for FUV) or light blue (for NUV) dashes. The sample with FUV-NUV  $>0$  includes stars cooler than  $\sim 20,000$  K, QSOs, and galaxies, as shown in Figures 4 and 5, and discussed by Bianchi et al. (2011a). Stars and QSOs are classified morphologically as “point-sources” (type=STAR) in the SDSS database, while most galaxies are classified as extended (type=GALAXY), as shown in Section 3. Sources with FUV-NUV  $<0$  are mostly hot stars, hot WDs in particular, except for some low-redshift QSOs with enhanced Ly $_{\alpha}$ . The bimodal distribution of sources in optical magnitudes mainly reflects the separation between stellar and extra-Galactic objects, as discussed by Bianchi et al. (2011a,b) and shown in Section 3. In spite of the SDSS DR14 magnitude depth<sup>12</sup> being  $\approx 2\text{--}3\text{mag}$  fainter than *GUVcat\_AIS*, GALEX can

---

<sup>12</sup>According to the online documentation for DR14 ([https://www.sdss.org/dr14/imaging/other\\_info/](https://www.sdss.org/dr14/imaging/other_info/)), the median  $5\text{-}\sigma$  depth for SDSS photometric observations, based on the formal errors from PSF photometry on point

detect the hottest stars (WDs) at further distances and with smaller radii than SDSS (Bianchi et al. (2011a) and Section 3).

### 3. Discussion. The Content of Astrophysical Sources in the Matched Catalogs.

To examine the content of different classes of astrophysical sources in the matched catalogs, we show color-color plots of the matched sources for representative samples at North Galactic latitudes, that are well covered by both Gaia and SDSS, and by *GUVcat\_AIS*, in Figures 4 to 7. Such plots allow us to separate different astrophysical objects, regardless of their distance, that is known only for the nearest sources, and would anyway introduce an additional uncertainty, not necessary (initially) for the purpose of broad source classification. We follow, as a starting point, the basic color-color plots used in our earlier studies (Bianchi et al. 2007, 2011a,b; Bianchi 2009), with additional models and details. We show color-color combinations, out of several possible, that best illustrate how and when different colors enable a clear separation (or not) of certain classes of sources, and of certain parameters ranges within these classes. These plots are an important first guide to possible uses of our catalogs, because, in extracting samples of selected candidate sources, it is also necessary to evaluate what other objects may intrude the selection, to estimate the purity of the sample, or - in other terms - the probability that the selected candidates belong to the intended class. Examples of scientific applications are the identification of Milky Way’s hot white dwarfs (WD), and in particular hot WDs with a less evolved (cooler, optically brighter) companion, by Bianchi et al. (2011a, 2018b) and Bianchi et al. (in preparation). Bianchi et al. (2011a) also published a quantitative comparison of hot-WD counts at different Galactic latitudes with Milky Way models, and showed that the

---

sources, is:  $u = 22.15$ ,  $g = 23.13$ ,  $r = 22.70$ ,  $i = 22.20$ , and  $z = 20.71$  ABmag

selection from the GALEX database reaches (optically elusive) hot WDs out to the Milky Way halo, and that extracted samples are sensitive to critical and yet poorly constrained aspects of stellar evolution, such as the Initial-Final Mass Relation (IFMR), that maps the final WD mass to the initial mass of its progenitor. Early model comparisons by Bianchi et al. (2011a) favoured IFMR with lower final masses, such as Weidemann (2000) IFMR. More recent results (Bianchi et al. 2018c) hinted that the binary fraction of observed WD samples is lower than that reported for unevolved stars, implying the possibility of a significant merging rate during binary evolution. But model-predicted source counts are sensitive to several ingredients, including assumptions on stellar evolution and on the geometry of stellar populations and interstellar dust (that affects observed magnitude distributions and stellar counts to given brightness limits) in the Milky Way. Comprehensive Milky Way model comparisons of the stellar samples in our matched catalogs are under way (dal Tio et al in preparation, Bianchi et al. in preparation, Million et al. in preparation).

Figures 4 to 7 illustrate the power of SED measurements extending to UV wavelengths for identifying and broadly classifying types of astrophysical sources that are either elusive or poorly characterized at longer wavelengths. In particular we recall that, for Milky Way-type extinction with  $R_V = 3.1$ , the GALEX FUV-NUV color is almost reddening-free (Bianchi 2011; Bianchi et al. 2017), as also shown by the reddening arrows drawn on the color-color plots in Figures 5, 7 and 8. Therefore, FUV-NUV is a direct, robust indicator of stellar  $T_{\text{eff}}$  (for  $R_V = 3.1$ -type extinction), while UV-optical or optical-only colors are highly affected by reddening, that must be accounted for in deriving stellar parameters from the observed SED, and carries an additional uncertainty. In addition, the plots illustrate the well-known greater sensitivity of UV data to the hottest  $T_{\text{eff}}$ s, to which optical colors are saturated, and to some other sources.

### 3.1. Point-like and extended sources

To separate point-like and extended sources in the matched catalogs, let’s first recall that SDSS imaging has a  $\sim 3\times$  higher resolution than GALEX imaging. Therefore, for *GUVmatch\_AISxSDSSdr14* sources, we use the SDSS tag “type”, which is in fact a classification based on the source morphology. A *type*=STAR source means point-like (at the SDSS resolution), and includes all stars and most if not all QSOs, while *type*=GALAXY selects extended sources, that are mostly galaxies, as shown in Figures 4 to 5.

Gaia DR2 does not include a similar morphological classification parameter. In DR2, photometry of extended sources is not specifically measured. Extended sources above the brightness limit are, however, included in the DR2 database; therefore, when measured with the same treatment as point sources, they result in a poor fit to the Gaia point-spread function (PSF). A measure of the fit quality, i.e., of how much a source departs from, or matches, the Gaia PSF, is given by the tags *astrometric\_excess\_noise* and *phot\_bp\_rp\_excess\_factor* (see e.g., Evans et al. (2018)). We mark with green dots in Figures 6 to 8 the Gaia sources with *astrometric\_excess\_noise*  $> 5$  and *phot\_bp\_rp\_excess\_factor*  $> 2$ , following Cheng et al. (private communication). The green dots cover sources in the galaxies’ color locus [NUV-G, BP-RP] (by analogy with the UV-SDSS color-color diagrams, and with model loci), and possibly also include some binaries (Section 3.3). In the NUV-G vs FUV-NUV diagrams, however, they are mostly “bluer” than the stellar sequence in NUV-G (not so in the NUV - SDSS-r color). We used in these plots the GALEX “best” magnitudes, that is, the measurements deemed by the GALEX pipeline to be the most adequate for each source. For extended sources, these are likely not aperture magnitudes. In the case of an extended source, GALEX and SDSS pipelines integrate over the entire object, while Gaia DR2 performs only a PSF fit, making GALEX-Gaia colors possibly inconsistent in such cases. Our catalog also includes GALEX aperture magnitudes with

varying aperture sizes; in the color-color plots we used the “best” magnitude throughout the sample for consistency. This criterion to identify extended sources in Gaia DR2 is explored here for the purpose of eliminating potentially extended sources from stellar samples.

### 3.2. Separating stars, QSOs, and galaxies

As mentioned, the match with SDSS offers, in addition to five optical bands extending the FUV, NUV GALEX measurements, also a morphological classification of the source shape (with respect to the PSF, thus limited to the SDSS  $\sim 1.4''$  resolution, which is higher than GALEX’s). In Figures 4 and 5 we color-coded the sources according to the SDSS classification of point-like sources (*type*=“STAR”) as blue dots, and extended sources (*type*=“GALAXY”) as black dots. Note that SDSS *type*=“STAR” refers to the source shape (sharpness), therefore it includes both stellar sources and extra-Galactic sources with a centrally peaked flux distribution, the latter being mostly QSOs.

The match of the UV sources with Gaia adds measurements in up to three optical bands, Gaia’s G, BP, and RP, and a parallax (and proper motion) measurement when a solution for these parameters was possible in Gaia DR2 (see Table 3 for the fraction of sources with parallax measurements). In the color-color plots of the matched Gaia sources (Figures 6 to 8), we marked with blue dots the sources with existing parallax measurements that are not negative (these indicate a failed solution) and have parallax error better than 20%.

The comparison of similar color combinations of UV-Gaia and UV-SDSS colors (Figures 4 to 8) shows similar distinct loci for stars, QSOs and galaxies, but marked differences in the relative source content. Most Gaia detections are point-like sources, and definitely more are stellar sources than QSOs; interestingly, Gaia also includes numerous cooler stars

with good measurements, that are readily eliminated in the SDSS sample by error cuts. Conversely, SDSS samples show a much higher relative number of extended sources, that are likely galaxies, shown as black dots in Figures 4 and 5. Also interesting in the Gaia sample are the numerous stars cooler than  $\sim 10,000\text{K}$ , showing a well-defined sequence of likely sub-solar metallicity giants or super-giants (as in the SDSS plots), mostly lacking parallax measurements, as can be expected because supergiants can be detected out to large distances at high Galactic latitudes. The plots also show two well-populated stellar sequences at lower  $T_{\text{eff}}$ , that mostly do have good parallax measurements, indicative of their proximity that allows them to be detected in *GUVcat\_AIS*, in spite of their cool temperatures and low intrinsic UV luminosity. As for the hot WDs, elusive at longer wavelengths but easily identified with the UV catalog, the two magenta sequences of WD model colors, with  $\log g = 7$  and  $9$  and  $T_{\text{eff}}$  between  $200,000\text{K}$  and  $15,000\text{K}$ , encompass a clear, well-defined sequence of Milky Way hot-WD candidates, that Bianchi et al. (2011a) found to have a purity of over 99%, by checking a subsample of about 4000 such sources with SDSS spectra.

The stellar models colors are from the Kurucz and TLUSTY model grids described by Bianchi (2009, 2011); Bianchi et al. (2007, 2011a). The QSO model colors, including colors computed from templates with  $\text{Ly}_\alpha$

### 3.3. Stellar binaries.

In some color-color plots we also show the loci of binaries composed of a hot WD and a cooler stellar companion. Examples are shown for WDs of  $T_{\text{eff}} = 100,000\text{K}$  and  $30,000\text{K}$  (purple and dark-pink models, respectively); for each  $T_{\text{eff}}$ , two WD radii,  $R_{WD} = 0.1R_\odot$  (with  $\log g = 6$ ) and  $R_{WD} = 0.02R_\odot$  (with  $\log g = 8$ ), are used to compute the binary composite magnitudes.  $T_{\text{eff}}$  and Radii for the cool-star companions (main sequence or giants) of

representative spectral types are taken from standard compilations. Given the scale of the plots, that span several magnitudes, using slightly different calibrations for spectral types will not produce an appreciable difference. When optical colors are involved, the addition of a cooler star displaces the source towards redder colors with respect to a single hot WD, as expected, the extent of this effect depends on the ratio of radii and  $T_{\text{eff}}$  between the stellar pair. Instead, the FUV-NUV color of the hot WD is hardly affected by cooler companions, again depending on how cool and how large the companion is. Such effects, initially pointed out by our earlier work, and used by Bianchi et al. (2018b) to select binaries for HST follow-up observations, enable selection of otherwise elusive binaries with a hot (and optically faint) WD. While the single-star sequences have a smooth, almost linear color progression with  $T_{\text{eff}}$ , the colors of binaries show a complex behaviour as a function of the cool companion’s  $T_{\text{eff}}$ , owing to the differing relative contribution of the two components in each filter. This can be understood, for example, by looking at examples of binary SEDs shown by Bianchi et al. (2018b) and Bianchi et al. (in preparation).

#### 4. Summary and Conclusions

We have matched the 83 million UV sources of *GUVcat\_AIS\_FOV055* (Bianchi et al. 2017, 2020a) with the optical databases Gaia DR2 and SDSS DR14. With a match radius of  $3''$ , we obtained:

- ***GUVmatch\_AISxGaiaDR2*.** 30,024,791 *GUVcat\_AIS* UV sources have 31,925,294 Gaia DR2 counterparts over the entire *GUVcat\_AIS* footprint, 26,275,572 of them have a parallax measurement, 18,588,139 with a parallax error  $\leq 30\%$ . FUV and NUV magnitudes are given in AB mag, and Gaia’s mags G, BP, RP in the Vega-mag system, to keep the values unaltered from the original respective databases. Conversions between AB and Vega mag systems are given in Table 2.

- *GUVmatch\_AISxSDSSdr14*. 22,207,563 *GUVcat\_AIS* sources have 23,310,532 SDSS DR14 counterparts, 10,167,460 of which are point-like, over a total overlapping sky area of  $\sim 11,100$  square degrees. All magnitudes FUV, NUV,  $u$ ,  $g$ ,  $r$ ,  $i$ ,  $z$  are given in the AB mag system.

The matched catalogs include all columns (tags) from *GUVcat\_AIS*, described in Table 8 of Bianchi et al. (2017), and all tags from the optical databases, described in their respective web sites, as well as additional tags to track multiple matches, defined in Table 1. Two *GUVcat* tags, *INLARGEOBJ* and *LARGEOBJSIZE*, flag sources that fall within the footprint of extended, complex objects, where the photometry of individual point sources may be compromised, or the flux may happen to be measured over different areas in different filters, making the colors misleading (see Bianchi et al. (2017)).

### *Artifacts*

We did not remove *GUVcat* sources with artifacts nor SDSS measurements with saturation flags or other warnings, because recipes to clean artifacts should be optimized according to each specific analysis and objective. Sources are included regardless of artifact flags, such as saturation or instrumental hot pixels, etc., also because an artifact may affect one filter but not the others. Some discussion about artifacts in GALEX photometry is given by Bianchi et al. (2017). The number of affected sources, however, is very small, therefore irrelevant for the purpose of our overview.

### *Multiple Matches*

A fraction of the *GUVcat* sources have more than one optical counterpart, on average  $\sim 6\%$  for Gaia DR2,  $\sim 5\%$  for SDSS DR14; this fraction can highly vary with magnitude range and Galactic latitude (see Bianchi et al. (2011a,b), and Tables 3 and 4). All

counterparts within the match radius are included in the catalogs, to enable tracking of multiple matches (Table 1). This is important for SED analysis, since a GALEX source that is resolved in two or more optical counterparts may include the composite flux of all of these counterparts, while the optical magnitude of the closest optical match will only include the flux from the one closest match, making UV–optical colors biased.

*Sky coverage. Source density*

To estimate, from source counts of an extracted sample, the average surface density of sources in the matched databases presented here, or that of *GUVcat*, SDSS, and Gaia, the areas of overlap between the footprint of the matched catalogs can be calculated for any region of the sky with the online interactive tool *AREAcats*<sup>13</sup> described by Bianchi et al. (2019) who also give area coverage at different Galactic latitudes for the matched catalogs, as well as for the individual databases, in their Table 1.

*Sources in the footprint of extended objects*

The number of matched sources, of subsets with single matches, as well as of those with parallax measurements for Gaia DR2, or with point-like classification and with existing spectra for SDSS, are given in Tables 3 and 4, by Galactic latitude and in total. In these tables we list counts both including all sources, and excluding those that fall within extended objects (large galaxies or clusters) larger than 30 arcmin, because sources in such complicated regions may have problematic identification and measurements (see Bianchi et al. (2017), in particular their Figure 5). Also, the flux of such sources maybe have been measured by GALEX, Gaia, and SDSS by integrating over very different profiles, making colors from combined datasets inconsistent and meaningless. Such sources require custom-made photometry, as shown by Bianchi et al. (2017).

---

<sup>13</sup><http://dolomiti.pha.jhu.edu/uvsky/area/AREAcats.php>

#### 4.1. How to access the Matched Catalogs and Related Tools

The matched catalogs can be downloaded (as fits or csv files) from the author web site <http://dolomiti.pha.jhu.edu/uvsky>, where *GUVcat*\_AIS is also available, as well as the AREAcats tool to calculate sky coverage of each matched catalog (and of the individual databases) in any chosen region of the sky. Both *GUVcat* and the cross-matched catalogs are also available at MAST as a High Level Science Product at <https://doi.org/10.17909/t9-pyxy-kg53>.

In addition, the catalogs can be conveniently browsed through the Casjobs interface at MAST (<http://mastweb.stsci.edu/gcasjobs/>), and will also be available from the SIMBAD Astronomical Database (CDS, Strasbourg) through VizieR; these sites also enable direct cross matching with additional catalogs residing in their respective repositories or uploaded by the user.

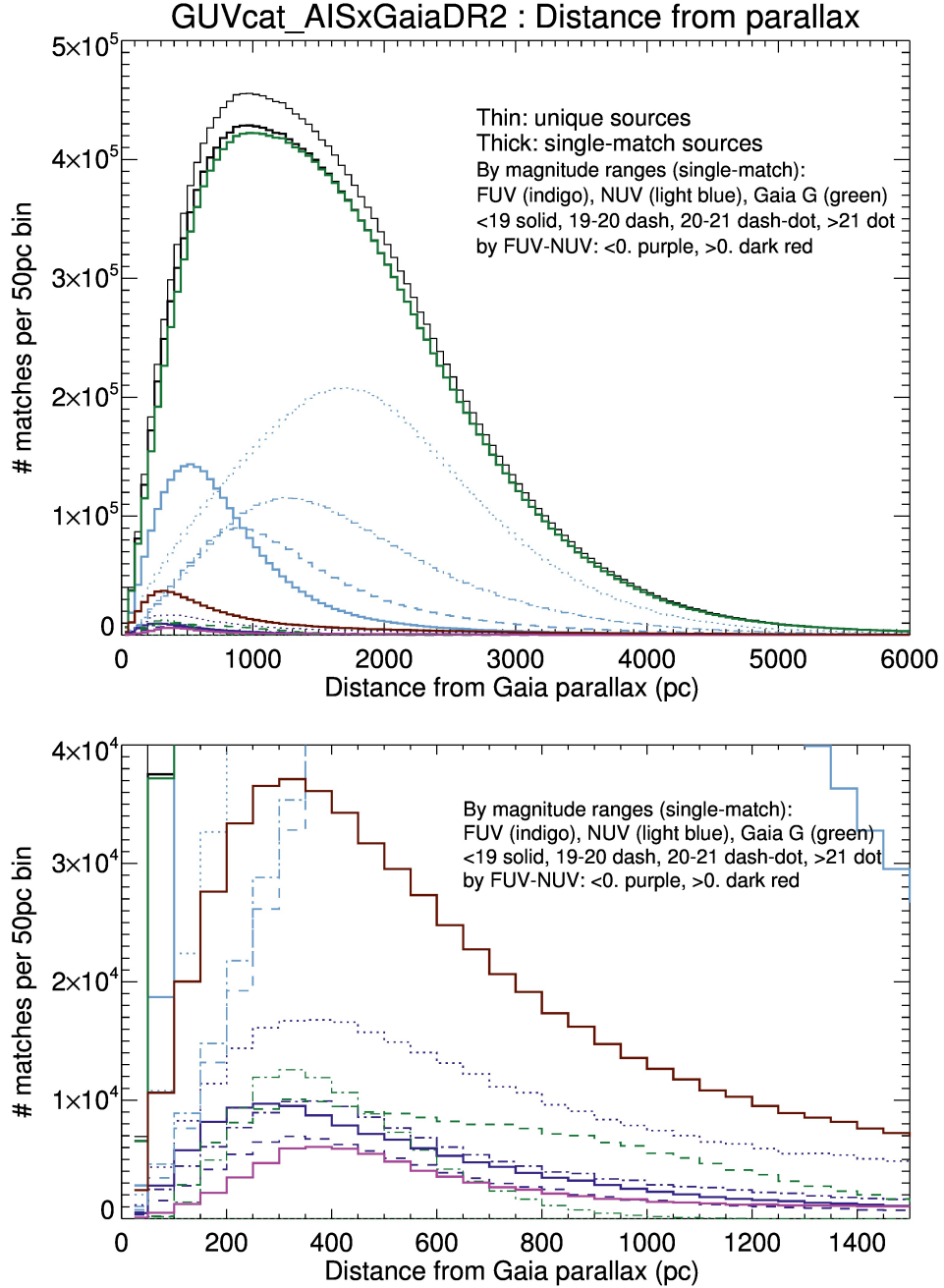


Fig. 2.— Distribution of distances (pc) derived from the Gaia parallax for the matched sources with parallax error less than 50%. The bottom panel is a zoom to distances  $<1500$  pc. Sources with FUV detection are about  $\sim 10\%$  of the NUV detections (see text) and are distributed over a range of magnitudes; Gaia parallax measurements are more numerous for sources with  $\text{FUV-NUV} > 0$ , that are relatively brighter at optical wavelengths than the hotter stars. The plot also illustrates the unique sensitivity of UV surveys to hot WDs, with respect to optical surveys (e.g., Bianchi et al. (2011a, 2018b)), and why Gaia’s WD sample

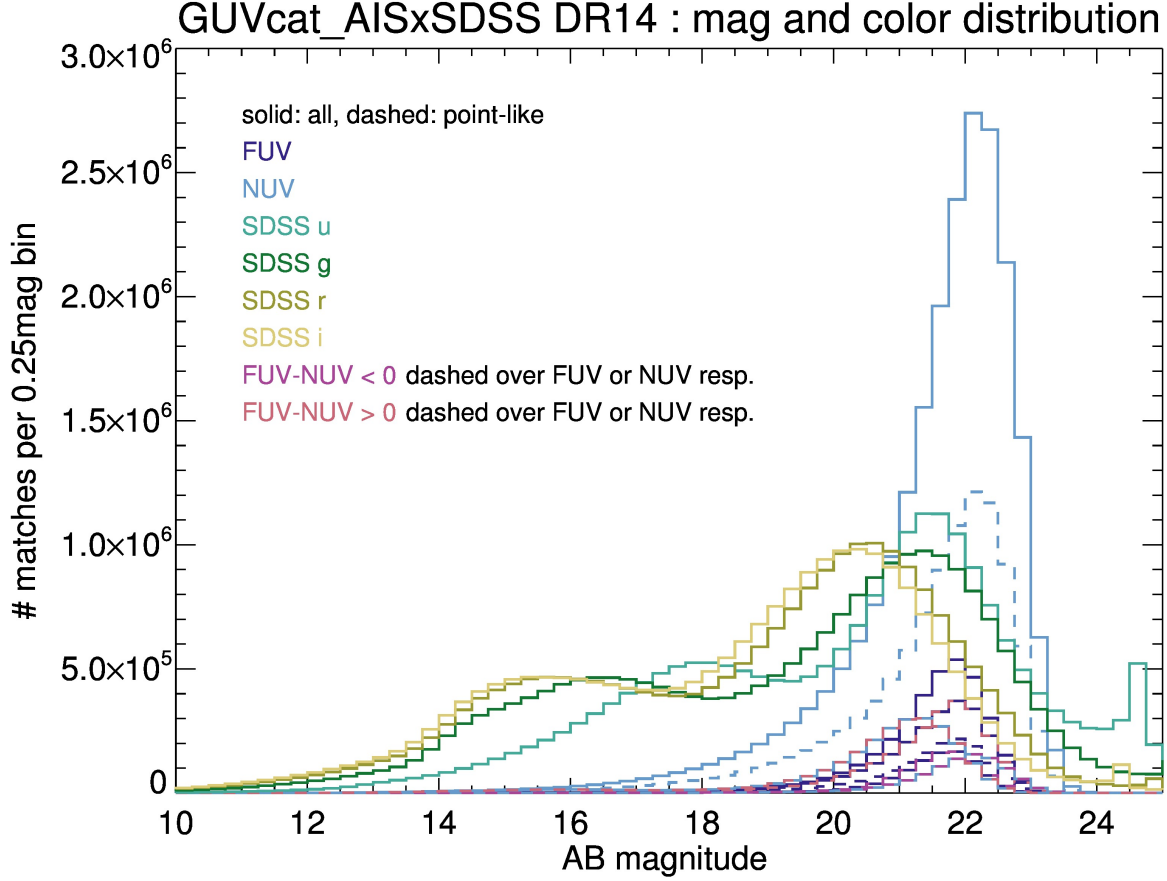


Fig. 3.— Distribution in FUV, NUV,  $u$ ,  $g$ ,  $r$ ,  $i$  magnitudes of the matched *GUVcat\_AIS* X SDSS DR14 sources, with color coding indicated in the legend. Dashed lines are for point-like sources, classified as such from SDSS imaging. We also plot FUV and NUV magnitude histograms of sources separated by  $\text{FUV-NUV} > 0$  and  $\text{FUV-NUV} < 0$ , with dashed light-red and fuchsia respectively, over indigo (FUV) and light-blue (NUV) histograms. Sources in objects larger than  $30'$  have been excluded. The bimodal distribution in optical passbands is mainly due to the presence of both Galactic and extra-Galactic populations, as seen in Figures 4 and 5.

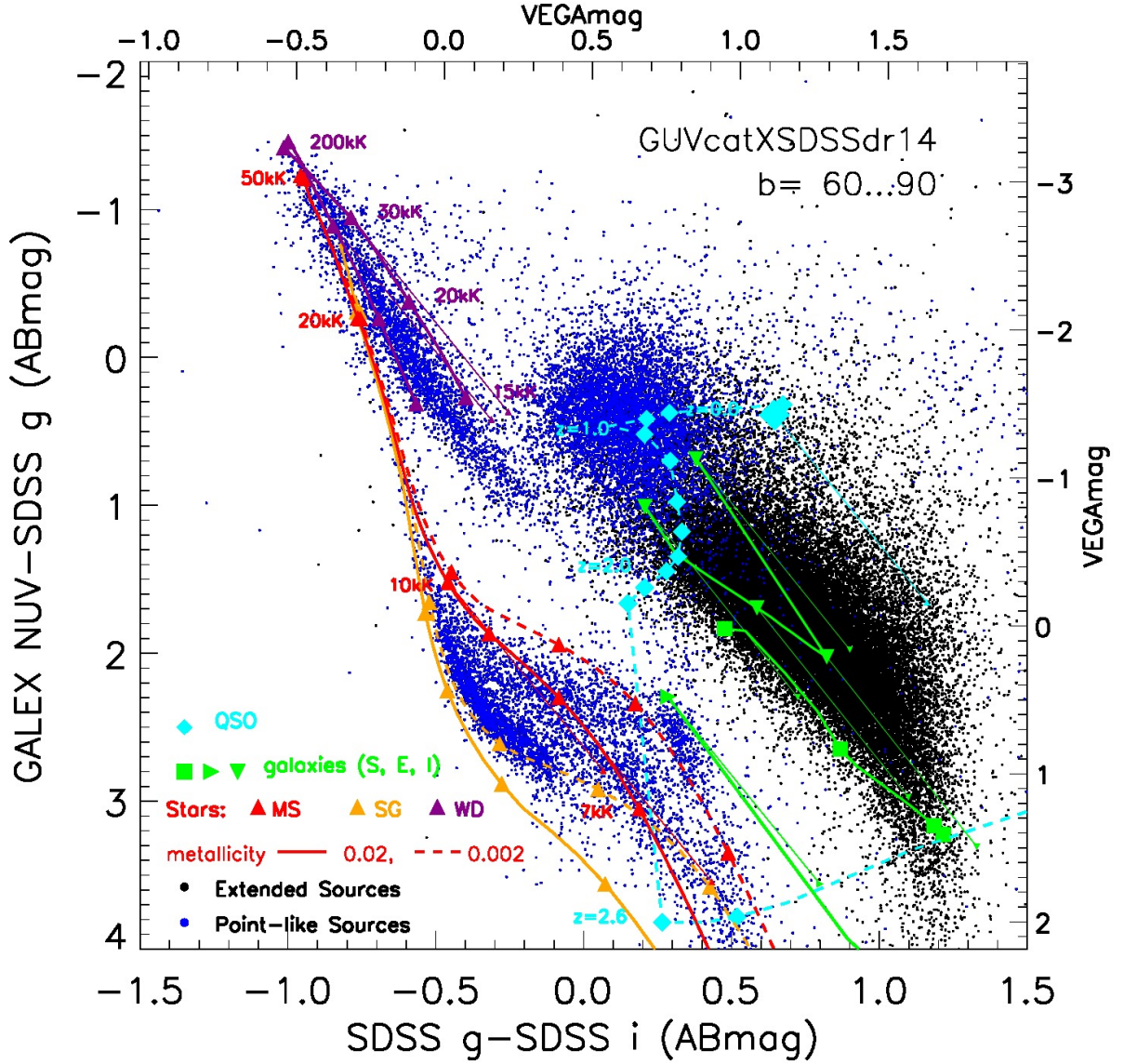


Fig. 4.— Color-color plot of *GUVmatch* AISxSDSSdr14 sources in the 60-90° North Galactic latitude range (dots; blue for point-like sources). Lines show model colors for stars of varying  $T_{\text{eff}}$  's (symbols mark  $T_{\text{eff}} = 50, 20, 10, 9, 8$  and  $7$  kK), galaxies of varying ages, and QSOs (redshift=0 (large cyan diamond), .2, .4, .6, 1.0, 1.2, 1.4, 1.8, 2.0, 2.2, 2.4, 2.6, 3.0, and 4.0), see legend and Section 3. Reddening vectors for  $E_{B-V}=0.3\text{mag}$  are shown as thin arrows starting from some unreddened model colors. Two purple  $T_{\text{eff}}$  sequences ( $T_{\text{eff}} = 200\text{kK}$  to  $15\text{kK}$ ) are pure-H WD colors for  $\log g=7$  and  $9$ . Numerous point-like sources within these sequences identify the Milky Way's hot WDs (Bianchi et al. 2011a). Point-like sources occupy the loci of stellar and QSO models, while galaxy model colors account for most extended sources. Other conspicuous stellar densities are seen for low-metallicity supergiants, detected out to large distances towards high Galactic latitudes, and main sequence stars of solar and sub-solar metallicity, that may constitute the thin and thick disk contributions. The actual number of stars cooler than  $\sim 8,000\text{K}$  steeply increases, but cooler sources, fainter in UV

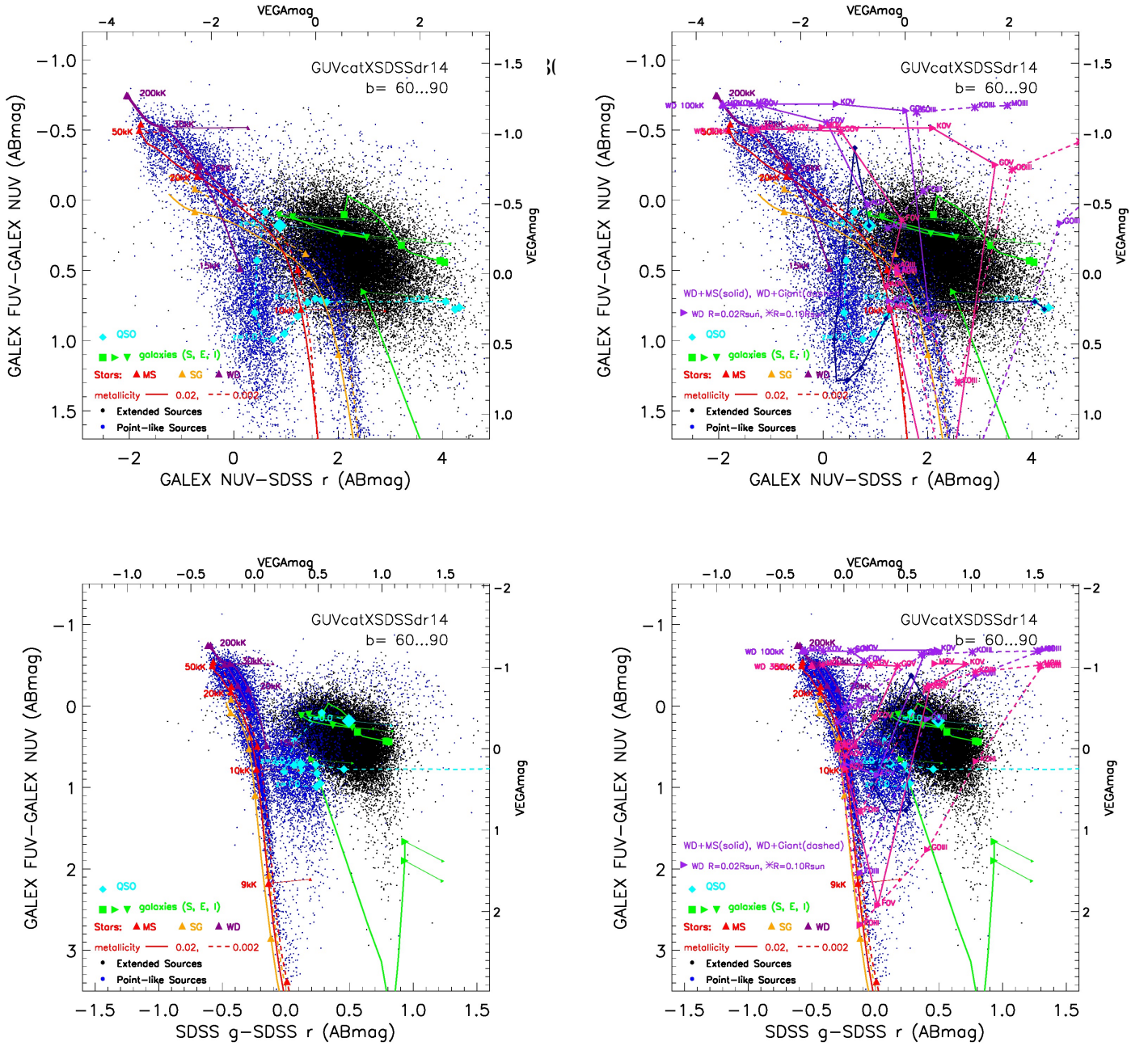


Fig. 5.— Color-color plots of *GUVmatch\_AISxSDSSdr14* sources, in the 60-90° N Galactic latitude, showing GALEX FUV-NUV. Models as described in the previous figure. In the right panels, composite model colors are added for WD+main sequence or WD+giant binaries, for WDs of  $T_{\text{eff}} = 100,000\text{K}$  (purple) and  $30,000\text{K}$  (dark pink), and radii of  $R_{\text{WD}} = 0.1R_{\odot}$  ( $\log g = 6$ ) and  $R_{\text{WD}} = 0.02R_{\odot}$  ( $\log g = 8$ ) with less evolved companions of representative spectral types. The colors of a single WD with these parameters are also shown for reference. Also, QSO templates with enhanced  $\text{Ly}_{\alpha}$ . The lower panels plot an optical color in the X-axis: note the different scale, and the much reduced sensitivity to discern object types, and stellar gravities, with respect to UV-optical colors (top plots). The lower plots show a wider FUV-NUV range, to include cooler sources, the top plots have a narrower FUV-NUV range to better see the hot-WD binaries.

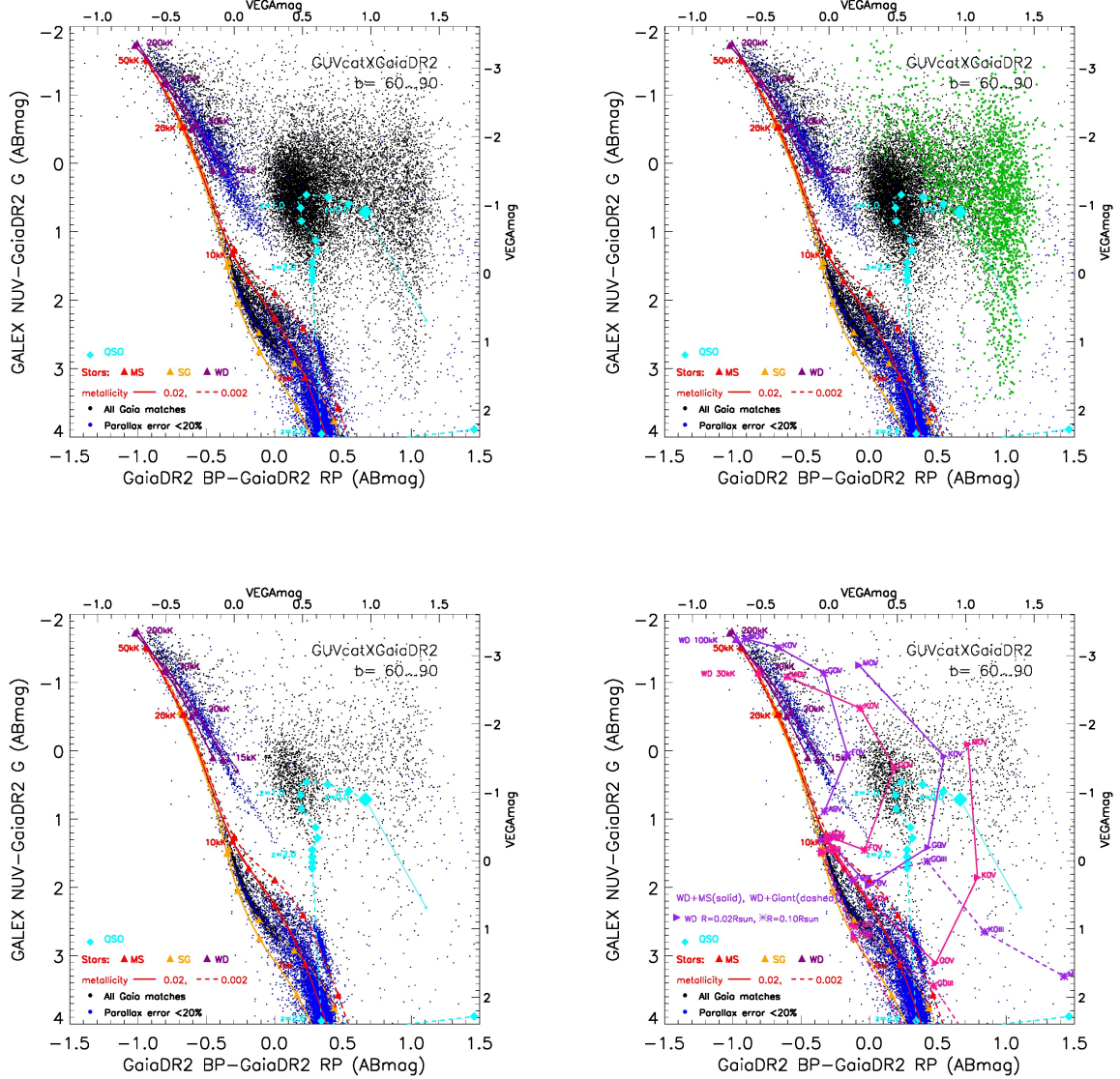


Fig. 6.— Top row: color-color diagrams of *GUVmatch\_AISxGaiaDR2* sources at  $b \geq 60^\circ$  N, with error  $< 0.1, 0.1, 0.2, 0.2$  mag in GALEX NUV, Gaia *G*, BP and RP mag. Blue dots mark sources with parallax error  $< 20\%$ . Green dots in the top-right panel mark “extended” sources (Section 3.1); they match the galaxies locus in previous plots (green dots are twice larger than others for evidence, as they are scant). Second row, left: more stringent error cuts (0.05, 0.05, 0.1, 0.1 mag) reduce the spread around the loci defined by model colors of object classes, as expected. It also reduces the relative number of extra-Galactic sources, that are typically fainter than Galactic objects, since progressively stringent error cuts translate into brighter magnitude limits (see e.g., Bianchi et al. (2007, 2011b)). The right-lower panel shows also composite colors for WD+main sequence or WD+giant binaries for WD’s  $T_{\text{eff}} = 100, 200\text{K}$  ( $\log g = 1$ ) and  $1, 20, 200\text{K}$  ( $\log g = 1$ ). Bottom:  $0.1\text{R}_{\text{eff}}$  ( $\log g = 6$ ) and  $0.02\text{R}_{\text{eff}}$  ( $\log g = 6$ ).

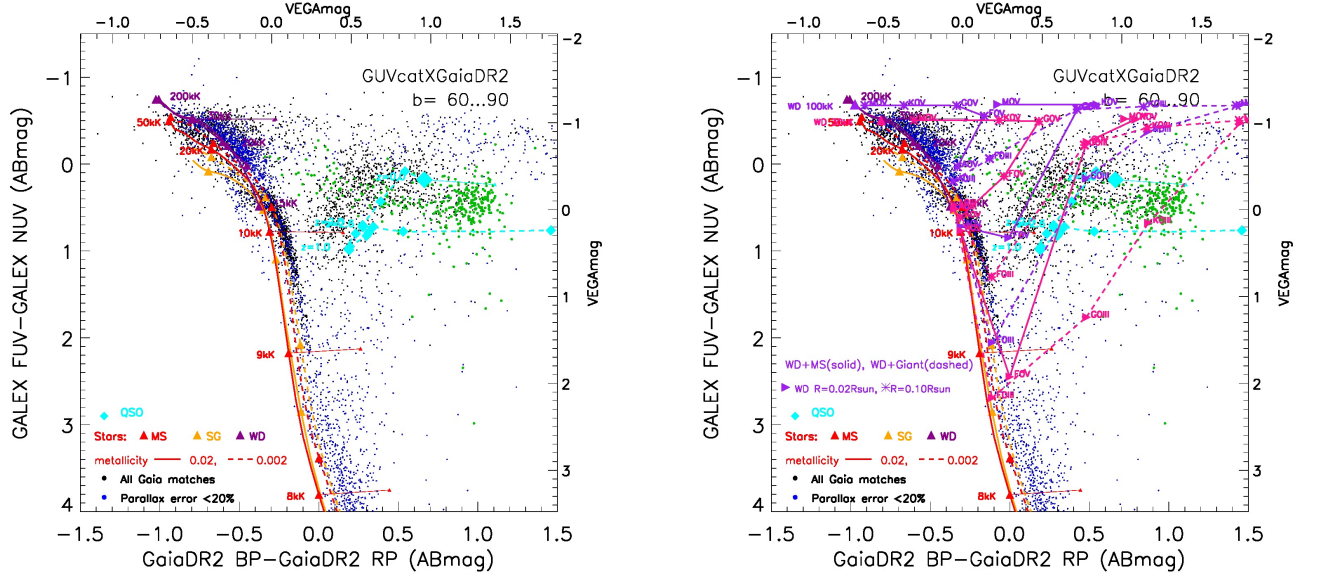


Fig. 7.— Same data and symbols as in the previous figure. Plots show the GALEX FUV-NUV color, that is essentially reddening-free for Milky Way-type extinction with  $R_V = 3.1$ : note the reddening arrows, almost horizontal, while in the previous figure the reddening runs almost parallel to the stellar models’  $T_{\text{eff}}$  sequence, making it impossible to discern  $[T_{\text{eff}}, E_{B-V}]$  effects, that are easily disentangled in this color combination. Error cuts here are  $<0.1, 0.1, 0.1, 0.2, 0.2\text{mag}$  for GALEX FUV, NUV, Gaia-G, BP and RP respectively. About one tenth of the NUV sources are also detected in FUV. As in previous figures, we show stellar and QSO model colors, with (right) and without (left) WD+cooler-star binaries for clarity. Blue points mark sources with parallax measurements (error  $<20\%$ ), and green dots (left panel) mark extended sources (i.e. sources with a “bad” Gaia PSF fit), likely galaxies.

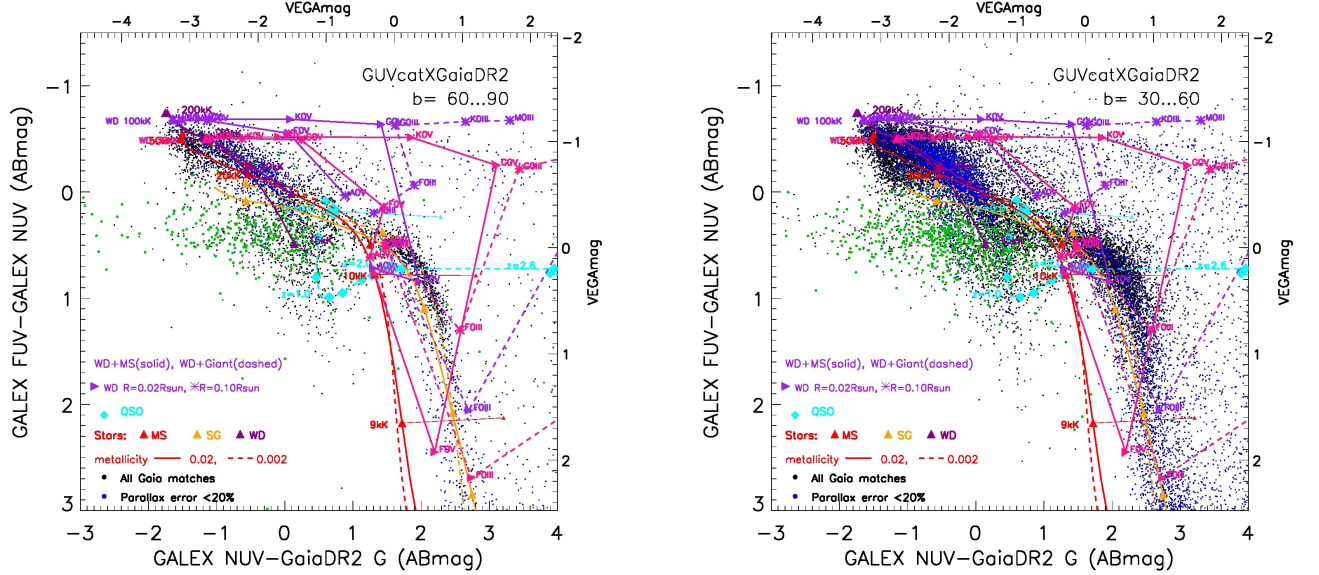


Fig. 8.— Data and symbols as in the previous figures, but this color combination separates red-shift $\sim 1$  QSOs from binaries with a hot WD, while the single-star sequences cross each other in the high  $T_{\text{eff}}$  regime, and at cooler  $T_{\text{eff}}$ 's they overlap with QSOs of red-shifts  $\sim 0$  and  $\sim 2$ ; the cooler ( $T_{\text{eff}} \sim 15,000\text{K}$ ) single WDs are close to the QSOs color locus. The left panel shows the sample at Galactic latitudes  $b=90\text{--}60^\circ$  N, as in the *GUVmatch*\_AISxSDSSdr14 plots; the right panel shows the  $b=30\text{--}60^\circ$  N range. Some of the sources extending to the left of the model sequences are probably galaxies, for which GALEX and Gaia photometry may be integrated over different areas, hence some probably meaningless very negative NUV -  $G$  values. Some may be emission-line nebulae (e.g., Gomez-Munoz et al. (2020)).

## REFERENCES

- Abolfathi, B. et al., 2018, arXiv:1707.09322v3 , DOI: 10.3847/1538-4365/aa9e8a
- Bianchi, L., Shiao, B., Thilker, D. 2020, in preparation (*GUVcat* revised)
- Bianchi, L., de la Vega, A., Shiao, B., & Souter, R. 2019, ApJS241, 14; DOI: 10.3847/1538-4365/aafec8 (*AREAcad*)
- Bianchi, L., de la Vega, A., Shiao, B., and Bohlin, R.C. 2018a, Ap&SS, 363: 56 ( DOI: 10.1007/s10509-018-3277-2 )
- Bianchi, L., Keller, G., Bohlin, R.C., Barstow, M., Casewell, S. 2018, Ap&SS, Vol. 363, Issue: 8, Article id: 166 (DOI: 10.1007/s10509-018-3369-z)
- Bianchi, L., et al. 2018c, contrib. to STScI Symp “The 21st Century H-R Diagram: The Power of Precision Photometry”,
- Bianchi, L., Shiao, B., Thilker, D. 2017, ApJS, 230, 24 [*GUVcat*]
- Bianchi, L. 2014, Ap&SS, 354, 103; DOI: 10.1007/s10509-014-1935-6
- Bianchi, L., Conti, A. and Shiao, B. 2014, J. Adv. Space Res., 53, 900 ( DOI:10.1016/j.asr.2013.07.045 ) ; arXiv 1312.3281 [*BCScat*]
- Bianchi, L. 2011, Ap&SS, 335, 51 ( DOI: 10.1007/s10509-011-0612-2 )
- Bianchi, L., Efremova, B., Herald, J., et al. 2011a, MNRAS, 411, 2770
- Bianchi, L., Herald, J., Efremova, B, et al. 2011b, Ap&SS, 335, 161
- Bianchi, L. 2009, Ap&SS, 320, 11
- Bianchi, L., Hutchings, J.B., Efremova, B., et al. 2009, AJ, 137, 3761

- Bianchi, L., Rodriguez-Merino, L., Viton, M., et al. 2007, ApJS, 173, 659
- Bianchi, L., Seibert, M., Zheng, W. et al. 2005, ApJ, 619, L27 ( DOI 10.1086/423710 )
- Brown, A. 2018, Proceedings of the International Astronomical Union, Vol. 12, p. 13  
(DOI:10.1017/S1743921317006664 )
- Chambers, K.C., Magnier, E.A., Metcalfe, N. et al. 2016, eprint arXiv:1612.05560v3
- Conti, A., Bianchi, L., Chopra, N., et al. 2014, J.ASR, 53, 967; DOI:  
10.1016/j.asr.2013.07.022
- dal Tio, P. et al. 2020, in preparation
- de la Vega, A. & Bianchi, L. 2018, ApJS, 238, 25 ( arXiv:1808.10455 )
- Evans, D.W., Riello, M., de Angeli, F., et al. 2018, A&A, 616, A4 (DOI:  
<https://doi.org/10.1051/0004-6361/201832756>)
- Gaia collaboration, Brown, A., Vallenari, A., et al. 2018, A&A, 616, A1 ( DOI:  
10.1051/0004-6361/201833051 )
- Gaia Collaboration, Babusiaux, C., van Leeuwen, F., 2018, A&A, 616, A10 ( DOI:  
10.1051/0004-6361/201832843 )
- Gomez-Munoz, M., Bianchi, L., Manchado-Torres, A., et al. 2020, A&A, in preparation
- Gunn, J. E., Carr, M. Rockosi, C., et al. 1998, AJ, 116, 3040
- Hutchings, J.B., & Bianchi, L. 2010a, AJ, 140, 1987
- Hutchings, J.B., & Bianchi, L. 2010b, AJ, 139, 630
- Lam, M.C., Hambly, N.C., Rowell, N. et al. 2019, MNRAS, 482, 715L (DOI: 10.1093/mn-  
ras/sty2710 )

- Marino, A., Bianchi, L., Rampazzo, R., et al. 2010, A&A, 511, 29
- Martin,D.C., et al. 2005, ApJ, 619, L1
- Million, C. et al. 2020, in preparation
- Morrissey, P., Conrow, T., Barlow, T., et al. 2007, ApJS, 173, 682
- Shoenrich, R., McMillan, P. & Eyer, L. 2019, arXiv:1902.02355, MNRAS487, 3568
- Smith, M., Bianchi, L., Shiao, B. 2014, AJ, 147, 159
- Sun, M., Jiang, B., Zhao, H. et al. 2018, ApJ, 861, 153
- Weidemann, V. 2000, A&A, 363, 647

We acknowledge support from NASA grants ADAP 80NSSC19K0527 and NNX17AF35G. We are grateful to Chase Million and David Thilker whom we often consult regarding GALEX data issues, for their always helpful answers. We thank especially Sihao Cheng for sharing results of his tests for Gaia pointlike/extended source classification, and Carla Cacciari and Anthony Brown for useful Gaia suggestions. We thank the referee for a careful and timely reading of the manuscript and helpful suggestions.

*Facilities:* GALEX, MAST

**ORCID iDs** Luciana Bianchi <https://orcid.org/0000-0001-7746-5461>

Table 3. Match *GUVcat\_AIS* x Gaia DR2: Statistics.<sup>a</sup>

<i>b</i> range	— # matches —			Multiple	Reverse	# with	# parallax error $\leq$		
	total matches	unique UV sources	single matches	matches # (%)	mult.mtc # (%)	parallax > 0.	20%	30%	50%
90...85	37166	36505	35854	651 (01.78%)	231 (00.63%)	28052	14913	16801	19433
	35904	35258	34622	1883 (01.80%)	226 (00.64%)	27110	14428	16247	18785
85...80	100390	98528	96683	1845 (01.87%)	614 (00.62%)	77305	43102	48179	55250
	96313	94504	92711	5817 (01.90%)	592 (00.63%)	74211	41308	46212	53033
80...75	179356	175393	171537	3856 (02.20%)	1103 (00.63%)	135580	74739	83665	95742
	177431	173856	170322	5071 (02.03%)	1050 (00.60%)	134661	74695	83612	95611
75...70	257933	252914	247945	4969 (01.96%)	1641 (00.65%)	195890	109940	123036	140652
	257933	252914	247945	4969 (01.96%)	1641 (00.65%)	195890	109940	123036	140652
70...65	315831	309644	303500	6144 (01.98%)	2128 (00.69%)	243584	137750	154507	176575
	315831	309644	303500	6144 (01.98%)	2128 (00.69%)	243584	137750	154507	176575
65...60	399685	391622	383621	8001 (02.04%)	2454 (00.63%)	311052	174758	196835	225933
	399685	391622	383621	8001 (02.04%)	2454 (00.63%)	311052	174758	196835	225933
60...55	522010	511189	500449	10740 (02.10%)	3250 (00.64%)	411617	234077	263893	302527
	522010	511189	500449	10740 (02.10%)	3250 (00.64%)	411617	234077	263893	302527
55...50	624112	610401	596798	13603 (02.23%)	4015 (00.66%)	502596	294695	332267	378942
	624112	610401	596798	13603 (02.23%)	4015 (00.66%)	502596	294695	332267	378942
50...45	800004	780943	762090	18853 (02.41%)	4913 (00.63%)	648602	381248	430671	492663
	799075	780198	761509	19434 (02.40%)	4912 (00.63%)	648052	381206	430600	492506
45...40	1014713	988382	962346	26036 (02.63%)	6844 (00.69%)	833513	497627	564076	644634
	1014713	988382	962346	26036 (02.63%)	6844 (00.69%)	833513	497627	564076	644634
40...35	1225590	1189097	1153071	36026 (03.03%)	8200 (00.69%)	1030336	629021	712460	811868
	1225564	1189072	1153047	36050 (03.03%)	8200 (00.69%)	1030313	629003	712442	811848
35...30	1520896	1468522	1416965	51557 (03.51%)	9809 (00.67%)	1296973	803431	911550	1036984
	1514477	1462291	1410921	57601 (03.51%)	9777 (00.67%)	1291457	799505	907277	1032306
30...25	1776297	1702747	1630787	71960 (04.23%)	10741 (00.63%)	1529460	975174	1104504	1248778
	1776297	1702747	1630787	71960 (04.23%)	10741 (00.63%)	1529460	975174	1104504	1248778
25...20	2039885	1937607	1838059	99548 (05.14%)	12302 (00.63%)	1764979	1159053	1311694	1473283
	2039010	1936791	1837297	100310 (05.14%)	12294 (00.63%)	1764192	1158378	1310989	1472546
20...15	2158395	2017830	1882301	135529 (06.72%)	11844 (00.59%)	1862541	1243181	1419498	1590218
	2150952	2011003	1876044	141786 (06.71%)	11798 (00.59%)	1856173	1238770	1414505	1584661
15...10	2096516	1887520	1693878	193642 (10.26%)	9503 (00.50%)	1751890	1171372	1350013	1516601
	2094443	1885668	1692235	195285 (10.26%)	9486 (00.50%)	1750186	1170159	1348664	1515128
10...5	882090	755647	646590	109057 (14.43%)	3366 (00.45%)	695727	463666	534592	602463
	882090	755647	646590	109057 (14.43%)	3366 (00.45%)	695727	463666	534592	602463
5...0	87028	75340	64843	10497 (13.93%)	279 (00.37%)	69380	49251	55684	61395
	86328	74733	64326	11014 (13.93%)	267 (00.36%)	68822	48885	55256	60915
0...-5	49725	45168	40808	4360 (09.65%)	118 (00.26%)	41924	32626	35483	38096
	49609	45068	40722	4446 (09.64%)	118 (00.26%)	41829	32546	35399	38009
-5...-10	441984	361938	293239	68699 (18.98%)	1620 (00.45%)	330249	245362	270611	293339
	440855	360908	292303	69635 (19.01%)	1619 (00.45%)	329272	244530	269727	292420
-10...-15	1584118	1363316	1164738	198578 (14.57%)	6422 (00.47%)	1254651	862572	970059	1077024
	1518247	1318639	1136577	226739 (13.81%)	6273 (00.48%)	1218184	846583	950736	1052981
-15...-20	2240184	2013886	1801929	211957 (10.52%)	10994 (00.55%)	1827972	1112037	1280319	1471552
	2147708	1938593	1741839	272047 (10.15%)	10606 (00.55%)	1763584	1081941	1244007	1426829

Table 3—Continued

$b$ range	— # matches —			Multiple matches # (%)	Reverse mult.mtc # (%)	# with parallax > 0.	# parallax error $\leq$		
	total matches	unique UV sources	single matches				20%	30%	50%
-20....-25	2022316	1894665	1771469	123196 (06.50%)	12572 (00.66%)	1722343	1062453	1218297	1394834
	2017783	1890402	1767458	127207 (06.50%)	12555 (00.66%)	1718829	1060188	1215735	1391943
-25....-30	1901493	1799945	1702177	97768 (05.43%)	13174 (00.73%)	1588977	947566	1087137	1250466
	1821160	1733444	1647945	152000 (04.93%)	12819 (00.74%)	1551262	936073	1074369	1235072
-30....-35	1792601	1671312	1561854	109458 (06.55%)	12097 (00.72%)	1409764	810207	927073	1067346
	1554521	1492890	1432521	238791 (04.04%)	10880 (00.73%)	1316529	790952	905488	1039274
-35....-40	1304958	1256064	1208755	47309 (03.77%)	10273 (00.82%)	1080221	652166	740868	845429
	1246228	1205727	1165906	90158 (03.30%)	10116 (00.84%)	1051101	642369	730139	832730
-40....-45	1085720	1046294	1008631	37663 (03.60%)	8031 (00.77%)	871944	514106	583229	666170
	1039739	1009051	978866	67428 (02.99%)	7893 (00.78%)	852042	511107	579242	659852
-45....-50	840241	816361	793077	23284 (02.85%)	7465 (00.91%)	679217	405908	458103	521787
	819236	798057	777129	39232 (02.62%)	7381 (00.92%)	668387	403591	455143	517496
-50....-55	659448	643777	628237	15540 (02.41%)	6489 (01.01%)	537432	327411	367814	416506
	657328	641713	626229	17548 (02.41%)	6472 (01.01%)	535709	326219	366532	415109
-55....-60	569548	556881	544316	12565 (02.26%)	4720 (00.85%)	458046	277814	311183	351388
	564344	551783	539323	17558 (02.26%)	4692 (00.85%)	453889	275039	308165	348101
-60....-65	426160	417042	407988	9054 (02.17%)	3120 (00.75%)	335976	201877	225698	254950
	426160	417042	407988	9054 (02.17%)	3120 (00.75%)	335976	201877	225698	254950
-65....-70	365868	358039	350339	7700 (02.15%)	3082 (00.86%)	286011	172493	191825	216321
	365868	358039	350339	7700 (02.15%)	3082 (00.86%)	286011	172493	191825	216321
-70....-75	268228	262655	257114	5541 (02.11%)	1898 (00.72%)	206818	123373	137482	155303
	268228	262655	257114	5541 (02.11%)	1898 (00.72%)	206818	123373	137482	155303
-75....-80	182037	178105	174204	3901 (02.19%)	1853 (01.04%)	139163	83798	92896	104394
	181590	177666	173773	4332 (02.19%)	1853 (01.04%)	138803	83590	92655	104123
-80....-85	117051	114601	112172	2429 (02.12%)	1291 (01.13%)	88674	52683	58365	65759
	116753	114307	111882	2719 (02.12%)	1291 (01.13%)	88421	52527	58190	65562
-85....-90	35717	34911	34123	788 (02.26%)	287 (00.82%)	27113	16055	17772	20024
	35717	34911	34123	788 (02.26%)	287 (00.82%)	27113	16055	17772	20024
90....-90	31925294	30024791	28242487	1782304 (05.94%)	198743 (00.66%)	26275572	16357505	18588139	21084629
	31283242	29516815	27847107	2177684 (05.66%)	195996 (00.66%)	25952375	16245077	18457818	20923942

<sup>a</sup>For each Galactic latitude range, the second row gives counts excluding sources in extended objects such as galaxies or stellar clusters larger than 30arcmin (see Bianchi et al. (2017)). Counts of sources with parallax measurements refer to the unique GUVcat sources ( $DISTANCERANK < 2$ ), not counting multiple matches to the same sources.

Table 4. Match *GUVcat\_AIS* x SDSS DR14: Statistics.<sup>a</sup>

<i>b</i> range	— # matches —			Multiple	Reverse	# Point-like		# SDSS spectra		
	total matches	unique UV sources	single matches	matches # (%)	mult.mtc # (%)	unique	FUV	unique	FUV	pnt
90...85	172873	164978	157341	7637 (04.63%)	1462 (00.89%)	41007	3261	7087	3441	2882
	167289	159632	152228	12750 (04.64%)	1437 (00.90%)	39610	3159	6882	3441	2812
85...80	397856	379062	360895	18167 (04.79%)	3457 (00.91%)	106514	8784	19467	10603	7720
	383207	365182	347758	31304 (04.77%)	3355 (00.92%)	102416	8440	18638	10603	7490
80...75	722113	687621	654348	33273 (04.84%)	5995 (00.87%)	190572	13285	35623	17533	14973
	721333	686895	653675	33946 (04.84%)	5965 (00.87%)	189951	13267	35523	17533	14877
75...70	1004931	959561	915741	43820 (04.57%)	8841 (00.92%)	276126	20058	52478	26814	22026
	1004931	959561	915741	43820 (04.57%)	8841 (00.92%)	276126	20058	52478	26814	22026
70...65	1165379	1112613	1061650	50963 (04.58%)	10366 (00.93%)	334967	24583	64906	31849	29336
	1165379	1112613	1061650	50963 (04.58%)	10366 (00.93%)	334967	24583	64906	31849	29336
65...60	1435902	1370927	1308205	62722 (04.58%)	12467 (00.91%)	424597	30268	75321	37077	34068
	1435902	1370927	1308205	62722 (04.58%)	12467 (00.91%)	424597	30268	75321	37077	34068
60...55	1618031	1548624	1481453	67171 (04.34%)	13564 (00.88%)	494329	33595	79899	40134	34414
	1618031	1548624	1481453	67171 (04.34%)	13564 (00.88%)	494329	33595	79899	40134	34414
55...50	1479736	1416075	1354386	61689 (04.36%)	13259 (00.94%)	511309	32796	72104	35390	33506
	1479736	1416075	1354386	61689 (04.36%)	13259 (00.94%)	511309	32796	72104	35390	33506
50...45	1601683	1530855	1462398	68457 (04.47%)	13769 (00.90%)	573799	35171	69282	33333	31588
	1601182	1530410	1462006	68849 (04.47%)	13768 (00.90%)	573412	35153	69273	33333	31584
45...40	1592536	1521609	1453149	68460 (04.50%)	14281 (00.94%)	640150	34762	61967	28776	29099
	1592536	1521609	1453149	68460 (04.50%)	14281 (00.94%)	640150	34762	61967	28776	29099
40...35	1389482	1325368	1263605	61763 (04.66%)	11499 (00.87%)	647806	34199	54402	24959	26887
	1389447	1325334	1263572	61796 (04.66%)	11499 (00.87%)	647782	34197	54401	24959	26887
35...30	1219365	1160754	1104645	56109 (04.83%)	8340 (00.72%)	645586	32207	35775	15961	18951
	1207012	1149117	1093687	67067 (04.82%)	8276 (00.72%)	639412	31808	35217	15961	18690
30...25	891847	849334	808569	40765 (04.80%)	6528 (00.77%)	513495	25324	23324	10344	12108
	891847	849334	808569	40765 (04.80%)	6528 (00.77%)	513495	25324	23324	10344	12108
25...20	755711	717308	680488	36820 (05.13%)	4680 (00.65%)	483062	24705	16988	6797	10043
	755711	717308	680488	36820 (05.13%)	4680 (00.65%)	483062	24705	16988	6797	10043
20...15	546600	516452	487622	28830 (05.58%)	2804 (00.54%)	410668	20412	5113	1113	4380
	546363	516230	487414	29038 (05.58%)	2804 (00.54%)	410479	20400	5109	1113	4377
15...10	270380	252959	236444	16515 (06.53%)	1206 (00.48%)	232277	10705	1424	216	1405
	270277	252859	236347	16612 (06.53%)	1206 (00.48%)	232182	10701	1423	216	1404
10...5	102469	95058	88071	6987 (07.35%)	465 (00.49%)	90803	5806	188	6	187
	102469	95058	88071	6987 (07.35%)	465 (00.49%)	90803	5806	188	6	187
5...0	4742	4458	4188	270 (06.06%)	14 (00.31%)	4230	443	0	0	0
	4742	4458	4188	270 (06.06%)	14 (00.31%)	4230	443	0	0	0
0...-5	0	0	0	0 (00.00%)	0 (00.00%)	0	0	0	0	0
	0	0	0	0 (00.00%)	0 (00.00%)	0	0	0	0	0
-5...-10	41107	37220	33648	3572 (09.60%)	201 (00.54%)	35622	1778	70	27	70
	41107	37220	33648	3572 (09.60%)	201 (00.54%)	35622	1778	70	27	70
-10...-15	279432	259483	240740	18743 (07.22%)	1248 (00.48%)	242300	9333	1122	127	1099
	279425	259476	240733	18750 (07.22%)	1248 (00.48%)	242293	9333	1122	127	1099
-15...-20	353430	330472	308636	21836 (06.61%)	1711 (00.52%)	291263	9781	1258	148	1232
	353429	330471	308635	21837 (06.61%)	1711 (00.52%)	291262	9781	1258	148	1232

Table 4—Continued

<i>b</i> range	— # matches —			Multiple matches # (%)	Reverse mult.mtc # (%)	# Point-like		# SDSS spectra		
	total matches	unique UV sources	single matches			unique	FUV	unique	FUV	pnt
-20...-25	550777	519144	488999	30145 (05.81%)	3671 (00.71%)	414541	15475	4422	905	3662
	549189	517742	487767	31377 (05.79%)	3667 (00.71%)	413455	15391	4422	905	3662
-25...-30	838755	795233	753743	41490 (05.22%)	5443 (00.68%)	542543	23395	11374	2923	7865
	837265	793810	752386	42847 (05.22%)	5433 (00.68%)	541721	23350	11344	2923	7842
-30...-35	846928	806816	768476	38340 (04.75%)	6211 (00.77%)	491805	23832	15389	4086	11032
	840856	801185	763258	43558 (04.73%)	6168 (00.77%)	488416	23284	15218	4086	10882
-35...-40	740300	706978	675090	31888 (04.51%)	6754 (00.96%)	374763	19144	23143	5953	17177
	740300	706978	675090	31888 (04.51%)	6754 (00.96%)	374763	19144	23143	5953	17177
-40...-45	593885	568458	544091	24367 (04.29%)	5218 (00.92%)	264591	15619	21078	6762	12516
	593885	568458	544091	24367 (04.29%)	5218 (00.92%)	264591	15619	21078	6762	12516
-45...-50	531705	506589	482601	23988 (04.74%)	5092 (01.01%)	213189	13257	19894	7570	9858
	531705	506589	482601	23988 (04.74%)	5092 (01.01%)	213189	13257	19894	7570	9858
-50...-55	490341	466454	443617	22837 (04.90%)	5209 (01.12%)	188403	12471	15447	5210	9582
	490341	466454	443617	22837 (04.90%)	5209 (01.12%)	188403	12471	15447	5210	9582
-55...-60	555550	529816	505064	24752 (04.67%)	7388 (01.39%)	175366	14785	25487	10287	14607
	555550	529816	505064	24752 (04.67%)	7388 (01.39%)	175366	14785	25487	10287	14607
-60...-65	495619	471024	447362	23662 (05.02%)	4956 (01.05%)	138722	12780	31257	14079	15920
	495619	471024	447362	23662 (05.02%)	4956 (01.05%)	138722	12780	31257	14079	15920
-65...-70	339441	324640	310346	14294 (04.40%)	3697 (01.14%)	97779	8445	9454	3211	6149
	339441	324640	310346	14294 (04.40%)	3697 (01.14%)	97779	8445	9454	3211	6149
-70...-75	176928	170122	163529	6593 (03.88%)	2036 (01.20%)	47308	4299	5095	2569	2264
	176928	170122	163529	6593 (03.88%)	2036 (01.20%)	47308	4299	5095	2569	2264
-75...-80	66080	63965	61904	2061 (03.22%)	550 (00.86%)	17753	1794	194	10	194
	66080	63965	61904	2061 (03.22%)	550 (00.86%)	17753	1794	194	10	194
-80...-85	35054	34072	33110	962 (02.82%)	315 (00.92%)	9097	884	192	9	192
	35054	34072	33110	962 (02.82%)	315 (00.92%)	9097	884	192	9	192
-85...-90	3564	3461	3360	101 (02.92%)	30 (00.87%)	1118	108	0	0	0
	3564	3461	3360	101 (02.92%)	30 (00.87%)	1118	108	0	0	0
90...-90	23310532	22207563	21147514	1060049 (04.77%)	192727 (00.87%)	10167460	577544	860224	388222	426992
	23267132	22166709	21109088	1098475 (04.77%)	192448 (00.87%)	10149170	575968	858316	388222	426154

<sup>a</sup>For each Galactic latitude range, the second row gives counts excluding sources in extended objects such as galaxies or stellar clusters larger than 30arcmin (see Bianchi et al. (2017)). Counts for sources with significant detection also in GALEX *FUV* are indicated with "FUV". "Point-like" sources are defined by the SDSS morphological classification of *TYPE*="STAR", that includes both galactic and extra-galactic point-like sources.